Proceedings of GT2006
ASME Turbo Expo 2006: Power for Land, Sea and Air
May 8-11, 2006, Barcelona, Spain

GT2006-90582

DESIGN AND TEST OF AN ASPIRATED COUNTER-ROTATING FAN

Jack L. Kerrebrock, Alan H. Epstein, Ali A. Merchant, Gerald R. Guenette, David Parker, Jean-Francois Onnee, Fritz Neumayer
Gas Turbine Laboratory
Massachusetts Institute of Technology
Cambridge, Massachusetts 02139, USA

John J. Adamczyk
NASA-Glenn Research Center
Cleveland, Ohio 44135, USA

Aamir Shabbir
University of Toledo
Toledo, Ohio 43606, USA

ABSTRACT

The design and test of a two-stage, vaneless, aspirated counter-rotating fan is presented in this paper. The fan nominal design objectives were a pressure ratio of 3:1 and adiabatic efficiency of 87%. A pressure ratio of 2.9 at 89% efficiency was measured in the tests. The configuration consists of a counter-swirl-producing inlet guide vane, followed by a high tip speed (1450 feet/sec) non-aspirated rotor, and a counter-rotating low speed (1150 feet/sec) aspirated rotor. The lower tip speed and lower solidity of the second rotor results in a blade loading above conventional limits, but enables a balance between the shock loss and viscous boundary layer loss, the latter of which can be controlled by aspiration. The aspiration slot on the second rotor suction surface extends from the hub up to 80% span, with a conventional tip clearance, and the bleed flow is discharged at the hub. The fan was tested in a short duration blowdown facility. Particular attention was given to the design of the instrumentation to obtain efficiency measurements within 0.5 percentage points. High response static pressure measurements were taken between the rotors and downstream of the fan to determine the stall behavior. Pressure ratio, mass flow, and efficiency on speedlines from 90% to 102% of the design speed are presented and discussed along with comparison to CFD predictions and design intent. The results presented here complement those presented earlier for two aspirated fan stages with tip shrouds, extending the validated design space for aspirated compressors to include designs with conventional unshrouded rotors and with inward removal of the aspirated flow.

INTRODUCTION

The work reported here is the latest element of a program being conducted by the MIT Gas Turbine Laboratory and its collaborators to develop and validate the technology for design of axial compressors that incorporates control of flow separation by aspiration (or suction) of the viscous flows at diffusion-limited locations. Prior to the work reported here, two aspirated single-stage fans were designed and tested. The first was a transport engine aspirated transonic fan stage, with a pressure ratio of 1.6 at a tip speed of only 750 feet/sec. It was designed and tested in the Blowdown Compressor at MIT as a first step in assessing the utility of aspiration for increasing stage loading [1]. A second, high tip speed, stage was designed and tested at NASA Glenn Research Center to assess the feasibility of similarly high loading at a tip speed of 1,500 ft/sec [2]. Rotor-tip shrouds were used in these designs for two reasons: first, to enable an assessment of the benefits of aspiration without the complications of tip clearance flows, and second, to provide a practical means in a first-stage configuration for transporting the aspirated flow outwards from the suction slots on the rotor blades to the rotor housing. Both fan stages validated the concept of aspiration by approximately doubling the stage work over that achievable in a similar stage without aspiration. They also validated the design system as a means for designing aspirated compressors with unusual design parameters, without prior empirical knowledge [3].

The new proposition addressed here is that aspiration offers additional benefits in application to compressors, either fans or cores, with counter-rotating blade rows, because of the high levels of work enabled by the swirl that enters the second rotor of a pair. This high work results in high aerodynamic loading and high Mach number in the second blade row of such counter-rotating pairs, both of which lead to diffusion problems that can be addressed with aspiration. The result is a potential for higher pressure ratios with fewer blade rows, hence either shorter and lighter compressors or compressors that meet unusual needs.

A configuration of special interest in this context is the counter-rotating fan studied here. It consists of a counter-swirl-producing inlet guide vane, followed by a high tip speed (1450 feet/sec) non-aspirated rotor, and a counter-rotating low speed (1150 feet/sec) aspirated rotor. There are no stators. The lower tip speed of the second rotor results in a blade loading above conventional limits, but delivers a good balance between the shock loss and viscous boundary layer loss, both of which can be controlled by aspiration. In the context of such counter-

rotating fans, viscous flow control via aspiration enables the design of high work, compact, and efficient compression systems that are not possible without such viscous flow control. Applications for such fans may be found in variable-cycle engines for multi-mission aircraft and in high-supersonic cruise aircraft [4,5].

Such counter-rotating configurations are not readily configured with tip shrouds, in part because of high temperatures in some potential applications, so the rotors were designed with conventional tip clearance and with provision for discharging the aspirated flow from the second rotor inward, rather than outward as in the previous aspirated stages. In addition to meeting the needs of potential applications, this choice enables a generic assessment of the feasibility of such inward discharge, which in general is desirable for energy recovery from the aspirated flow.

To minimize the time and cost of testing the counter-rotating fan, which will be described in more detail below, the evaluation has been carried out in a short test duration blowdown facility at MIT. As discussed in more detail below, the several hundred milliseconds test duration of this facility enables evaluation of the performance of the compressor in terms of its pressure ratio, mass flow, and efficiency by means of conventional instrumentation such as is used in continuously operating test facilities. The key requirement is for thermocouple response fast enough to achieve essentially steady measurements during the blowdown time. All temperature measurements reported here meet this requirement. Therefore the measurements of pressure ratio, mass flow, and efficiency are directly comparable to those that would be obtained for the same configuration in a steady test facility.

Efficiency being an important component of such a comparison, it is important to note that in this paper, to isolate the effect of aspiration on efficiency, we quote the through-flow adiabatic efficiency. Specifically, this is the adiabatic efficiency of the compressor based on the stator (or rotor) outflow. This through-flow efficiency includes the effects of shock losses in the core flow and viscous losses that influence the entropy of the outflow of the compressor. It does not embrace the effects of losses that raise the entropy of the aspirated flow, or the work associated with it. The overall impact of these (secondary) effects of aspiration can be properly quantified only in the context of a complete engine design, in which the handling of the aspirated flows is explicated. Merchant *et al*. [6] qualitatively explore the key issues of aspiration on the engine efficiency, and Kirtley *et al*. [7] has also examined the impact of flow control in the context of efficiency of multistage compressors. This said, we do comment on the impact of bleed on efficiency later in the paper.

The structure of the remainder of this paper is as follows. The aerodynamic design is summarized first, followed by a brief description of the mechanical design of the stage and facility. The overall compressor performance is discussed and compared with the predictions of multi-stage CFD analyses. The operability and off-design behavior is discussed briefly. Lastly, the important conclusions and implications of the results of the test program are enumerated.

AERODYNAMIC DESIGN

The nominal design objectives for the counter-rotating fan based on engine concept studies are presented in Table 1. The desired pressure ratio was 3:1 with an adiabatic efficiency goal of 87%. The RPM ratio for the rotors was approximately 0.8, and the corresponding tip speed ranges are given in the table. The design point stall margin was 20%. An inlet guide vane was included in the engine concept for off-design operation, and this was exploited in optimizing the performance at the design point. The exit swirl from the second rotor was constrained to less than 15 deg, consistent with either a mechanical strut that could remove the residual swirl or entry into a core.

Table 1: Nominal fan design objectives

Pressure Ratio	3:1
Adiabatic Efficiency	87%
Rotor 1 Speed Range	1400-1500 ft/sec
Rotor 2 Speed Range	1100-1250 ft/sec
Specific Flow	41.5 lbm/sec/ft^2
Exit Mach No.	0.5
Exit Swirl Angle	<15 deg

In contrast to the design of a conventional fan, this design was complicated by the introduction of the second independent rotor with its tip speed and work coefficient as additional design variables. The absence of a vane between the rotors added further complexity to the design effort due to the very high relative supersonic Mach numbers into the second rotor.

In order to clarify the roles of design variables such as rotor speed ratio, a preliminary design study and optimization of design parameters was performed using a one-dimensional model of the fan. The model included compressibility, area change, shock loss, and viscous loss models. Parametric studies were carried out using rotor speeds, rotor work coefficients, and inlet guide vane swirl as variables to explore the design space. Finally, a constrained optimization was performed to arrive at the optimum values for the preliminary design.

The parametric study showed that the speed of the second rotor has a strong impact on the efficiency, mainly due to the shock loss at high relative Mach numbers at the rotor face (Figure 1). The speed of the first rotor has a relatively small impact on the overall efficiency, since the average Mach number varies only from 0.95 to 1.15 over the speed range. In contrast, the average Mach number in the second rotor varies from 1.4 to 1.6. Note that this variation was calculated without any counter-swirl in the first rotor. Lowering the blade speed of the second rotor to manage the Mach number, while maintaining the design pressure ratio, results in a higher work coefficient and blade loading than is found in conventional supersonic rotors.

Adding counter-swirl via the inlet guide vane increases the relative Mach number into the first rotor, but lowers the relative Mach number into the second rotor. As shown in Figure 1b, the efficiency reaches a peak at about 15 degrees of counter-swirl. A linear counter-swirl variation from 10 degrees at the hub to 0 degrees at the tip was used in the final design.

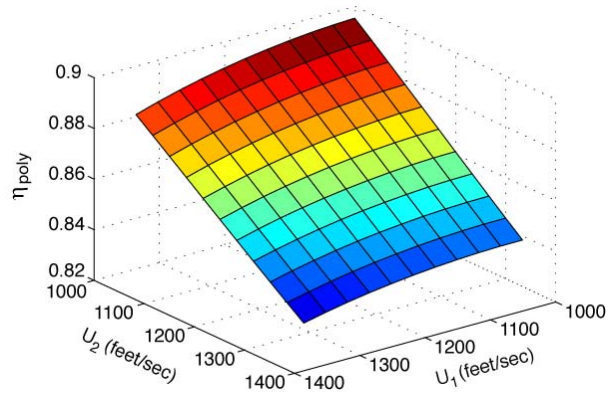

(a) Efficiency variation with Rotor 1 and 2 tip speeds.

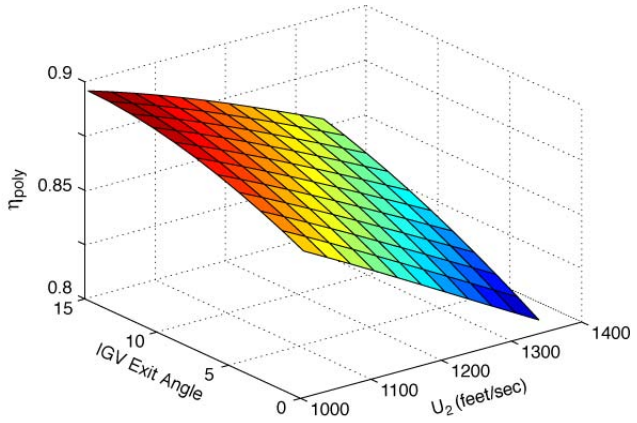

(b) Efficiency variation with IGV counter-swirl and Rotor 2 tip speed.

Figure 1: Design calculations of the effect of rotor speeds and IGV counter-swirl on fan efficiency.

The optimized 1D design was used as the starting point for a coupled axisymmetric-quasi-3D design of the fan. Fan design parameters are shown in Table 2. The flowpath was designed to provide sufficient flow contraction to maintain an acceptable meanline axial velocity decrease. The inlet radius ratio was constrained by the test facility and the exit radius ratio was selected to achieve an exit Mach number of 0.5 at design conditions. The casing flowpath was sloped 2% across each rotor to unload the tip sections, especially that of the second rotor. The aerodynamic design of the blades was carried out using the aspirated blade design system described in Merchant [3].

Three-dimensional viscous analysis of the stage, using the multi-stage average passage APNASA code developed by Adamczyk [8], was a critical component in the design process. The high supersonic Mach numbers in the blade rows, close blade row spacing, coupled with the very high blade loading demanded more accurate blade row matching than is possible with mixing-plane approaches. While the blade design was carried out using the quasi-3D design system, modifications to blade geometry, primarily incidence changes, were made using information extracted from the 3D APNASA solution.

Table 2: Fan aerodynamic design parameters

Rotor Speeds	1450 fps	1150 fps
Work Coefficient	0.34	0.5
Diffusion Factor	0.48	0.55
Hub Relative Mach	1.0	1.3
Tip Relative Mach	1.5	1.45
Blade Count	20	29
Avg. Solidity	1.9	1.7
Avg. Aspect Ratio	1.6	1.75
Inlet Radius Ratio	0.5	0.65

The predicted nominal design point performance for the fan calculated using APNASA is shown in Table 3. The tip clearances for the rotors were approximately 0.6% (Rotor 1) and 0.9% (Rotor 2) of the tip chord. The fan predictions exceeded the efficiency goal by 1.2% at the design pressure ratio, and achieved a peak adiabatic efficiency of 89% at a pressure ratio of 3.16.

Table 3: CFD predicted nominal design point performance

	Rotor 1	**Rotor 2**	**Overall**
Pressure Ratio	1.92	1.6	3.02
Adiab. Efficiency %	91.2	86.6	88.2
Poly. Efficiency %	92.3	87.5	90.0
Aspiration %	0	1.0	1.0

It is interesting to compare the design parameters of the two rotors shown in Table 2. Although the first rotor parameters are in the range of conventional supersonic fans, the aspect ratio is higher due to a lower average solidity [9]. The average Mach number of the first rotor is also higher than for conventional fans due to the counter-swirl from the inlet guide vane. The second rotor has a 40% higher work coefficient and 20% higher average Mach number than the first rotor. The average solidity is also significantly lower than for conventional fans. This is due to a combination of reduced blade count and reduced chord length, both enabled by aspiration.

The detailed design process revealed that a started shock system in the second rotor was critical to meeting the performance goals. This was complicated by three issues: 1) excessive hub boundary layer growth at the shock impingement location leading to shock unstart at the hub, 2) achieving the correct blade throat margin to maintain started flow at design and part speed conditions, and 3) managing the blade blockage by keeping the blade count low while maintaining sufficient solidity to meet the high loading requirement. Aspiration was critical in addressing these issues. First, the position of the passage shock was stabilized by aspiration. This approach has been utilized in the form of "shock traps" in supersonic inlets and was also incorporated in previous aspirated compressors [6]. Second, aspiration enabled blade designs with 20% lower solidity at diffusion factors of 0.55. This resulted in reduced blade blockage and enabled a blade design with sufficient throat margin [10]. Increasing the throat margin results in a stronger shock system that could be tolerated with aspiration.

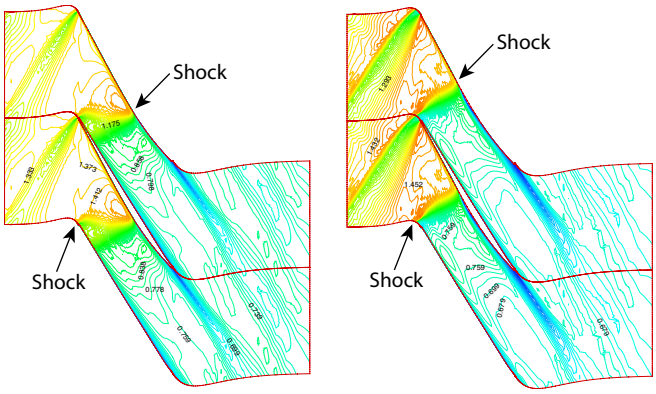

(a) Peak efficiency **(b) Peak pressure ratio**

Figure 2: Contours of Mach number in Rotor 2 at mid-span.

To illustrate the shock locations and boundary layer thicknesses, Figure 2 presents relative Mach number contours at mid-span, from the APNASA calculation. The peak efficiency point (Figure 2a) has a started shock and a well-attached suction side boundary layer, and the peak pressure ratio point is the last computed CFD point, which shows a spilled shock system. A mid-span quasi-3D analysis of the impact of aspiration on the characteristics of the rotor showed that 1% aspiration resulted in a gain of 2 percentage points in efficiency and 6% in pressure ratio before shock unstart.

Figure 3 shows the predicted design speed pressure ratio and adiabatic efficiency with different levels of aspiration (percent of inlet mass flow). The mass flow variation at 0% aspiration indicates that both rotors are unchoked at the computed points. The peak pressure ratio is 3.08 and the peak efficiency potential is 84%. Comparing the speedlines at 0.5% and 1% aspiration, there is little difference in the peak efficiency, but the pressure ratio at 0.5% aspiration at which the speedline rolls off is 4% lower than at 1% aspiration. The predicted stall margin potential based on the last computed CFD point, calculated using the method in Wadia *et al*. [9], is 15% at the design bleed, 11% at 0.5% bleed, and 6% at 0% bleed.

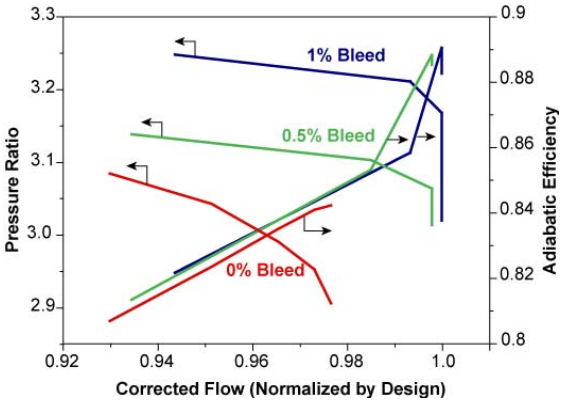

Figure 3: Predicted fan design speed pressure ratio and efficiency at different levels of aspiration.

EXPERIMENT DESCRIPTION

The theory and first application of blowdown compressor testing is described in Kerrebrock [11]. This blowdown facility is shown in Figure 4, and its test section details in Figure 5. The facility consists of a supply tank, initially separated by a fast-acting annular valve from the counter-rotating compressor stages and the dump tank into which they discharge. A choked perforated plate placed between the valve and test section was used to tailor the transient characteristics of the facility to the flow requirements of the compressor. A choked, adjustable area throttle downstream of the stage set the operating point. For this experiment, a sufficient the test time was required to permit accurate measurements of temperatures at the entrance to and exit from the compressor. In this facility, the measurement uncertainty of efficiency is dominated by temperature rise uncertainty. For these experiments, the target for efficiency measurement was 0.5%, which requires measurement of the temperature rise to about the same accuracy. Such instrumentation had been demonstrated for blowdown turbine stage testing [12]. This established a 100 ms test time requirement. This short test time precludes aeromechanical problems with the test hardware over the life of a typical test program.

A characteristic of blowdown compressors as used at MIT is that the decrease of the temperature of the gas in the supply tank during the test time is matched by slowing of the rotor, which is driven by its angular inertia, so that the Mach number of rotation is nearly constant during the blowdown. The relatively long test time of these experiments required the addition of a flywheel on each of the spindles carrying the rotors.

The test section, consisting of the two rotors, each on an independent, electric motor-driven spindle, is shown in Figure 5. The need to provide sufficient inertia to drive these high work stages for the required test time sized the flywheel inertia. The desire to keep the rotating systems' critical speeds above their operating range thus imposed a minimum hub-to-tip ratio on the first rotor of about 0.5. The tungsten flywheels, around which the test section was designed, failed during proof test, necessitating their replacement with maraging steel units. The resultant reduction in flywheel inertia was compensated for by reducing the inlet pressure and thus the test Reynolds number by about 20%.

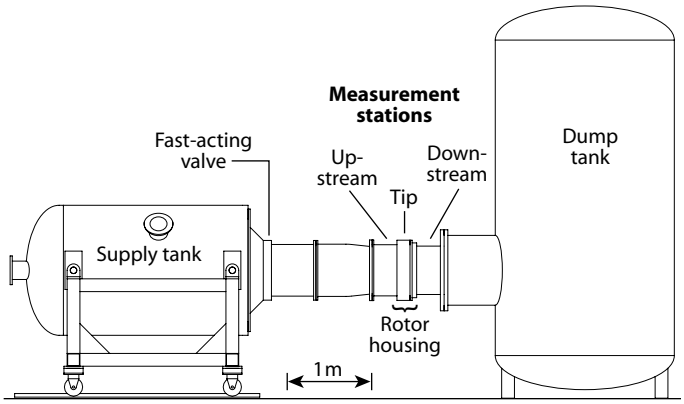

Figure 4: Blowdown facility.

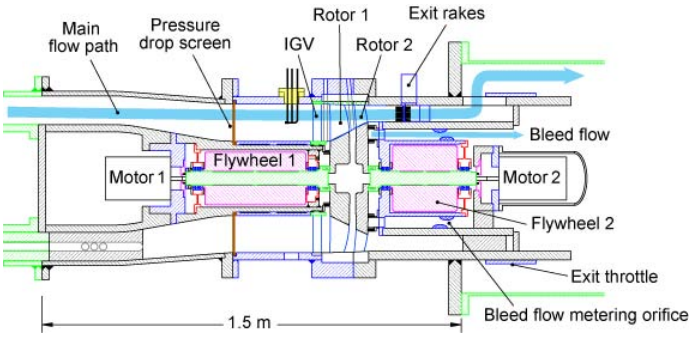

Figure 5: Counter-rotating fan test section.

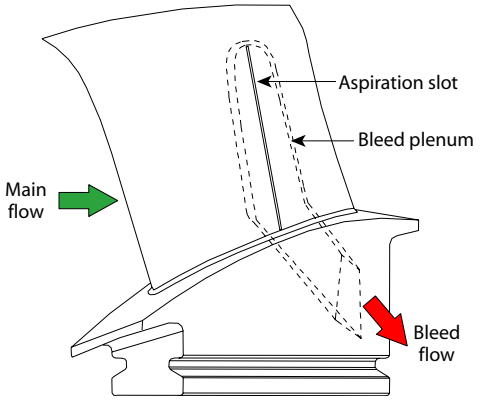

Figure 6: Aspiration passage geometry in Rotor 2.

The first rotor is an integrated bladed steel disk. The second rotor dovetails steel blades to a steel disk. Steel was chosen for the second rotor blades to ease construction of the hollow airfoils. They were fabricated by milling a bleed passage within a partially finished blade, e-beam welding on a cover, and then finish machining. The bleed air is removed through a passage electro-discharge-machined through the rear blade tang as shown in Figure 6. The bleed flowpath was designed to choke the suction surface slot so as to establish the bleed flow rate. Details of the mechanical design were given by Parker [13].

Primary performance instrumentation consisted of static and total pressure probes and rakes, and stagnation temperature rakes located ahead of the first rotor and behind the second rotor. (This test-section did not have torque-meters.) Also, high frequency response wall static pressure transducers were located in the casing between the two rotors, and just downstream of the second rotor. The rotor speeds and tank pressures were recorded as well. The pressure across an annular orifice in the bleed flowpath downstream of the second rotor was measured to monitor the aspirated bleed flow but programmatic constraints precluded proper bleed flowpath calibration so the bleed flow estimates in this paper are from the bleed flowpath design CFD calculations.

For these tests, a gas mixture of CO_2 and Argon with a ratio of specific heats, γ, of 1.4 was used in place of air to reduce the speed of sound (and thus mechanical stresses) while maintaining aerodynamic and thermodynamic similarity with air at flight conditions. During data reduction, the mixture was treated as real gas with properties estimated from NIST data (γ changes by about 3% from the stage inlet to outlet). Details of the construction and calibration of the instrumentation along with the test error analysis were given by Onnee [14].

BLOWDOWN OPERATION

Insofar as we are aware, this is the first two-rotor configuration tested in a transient facility and some effort was required to realize the desired test behavior. Given fixed rotor inertia and geometry, the operating condition of the fan during the test time is set by the initial rotor speeds, the supply tank pressure and temperature, and throttle areas downstream of the second rotor and in the bleed flowpath (which are adjustable). Figure 7 shows a typical simulated test time history. While the pressures and temperatures vary during the test, the pressure and temperature ratios across the stage remain close to constant for a sufficient period to enable accurate measurement of the fan performance. The useful test time is after the initial startup transient, from 250 ms to approximately 350 ms. The rise of the dump tank pressure then results in unchoking of the throttle and eventual stall of the fan.

The corrected flow is derived from a survey of the stagnation and static pressures upstream of the first rotor, and is essentially a measure of the Mach number at that point. Corrected speed is derived from the measured rotative speed and the measured temperature upstream of the first rotor. All of the measured values, including the rotative speed, are variable in time during the run, so a point on the map is defined by selecting a time near the middle of the test time, when the rotative and flow Mach numbers are nearly constant, and calculating the operating point from the values measured at that time. Typical variation in corrected speed and weight flow during the nominal 100 ms test time is shown in Figure 8, which shows a variation of less than ±0.5% in corrected speed and ±1.6% in corrected flow.

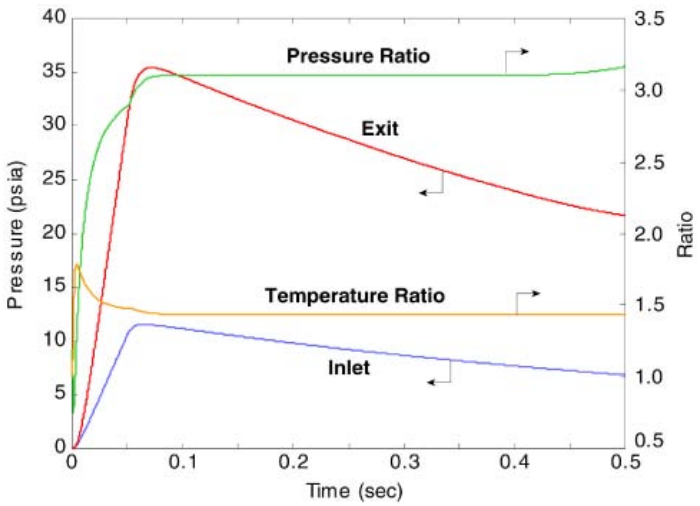

Figure 7: Typical variation of flow conditions during a blowdown test.

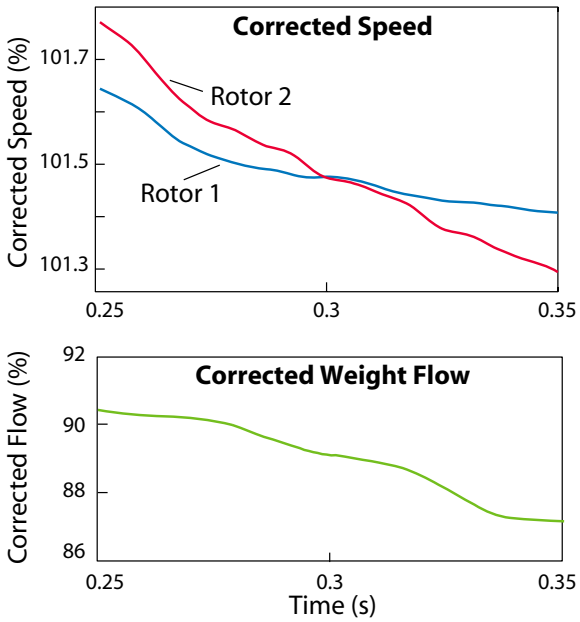

Figure 8: Measured corrected rotor speed variations.

After this 100 ms test period, the operating point changes as the throttles unchoke, resulting in the fan stalling after several hundred milliseconds. Conceptually, data from this period could be used to map out the stage behavior over the operating line followed. Such analysis has yet to be done however, and all data reported herein is that averaged over the 100 ms matched test time.

RESULTS AND DISCUSSION

In this section we present and discuss the overall fan performance map. The experimental results are compared and reconciled with CFD calculations carried out using APNASA. The stall behavior of the fan is also discussed from a first principles analysis. In order to assist in understanding the measured performance of the fan, a simple one-dimensional model, which includes shock loss, diffusion loss, and a coupling of the mass flow to the rotor speed (assuming that both rotors operate with a unique incidence condition), was used. The model was calibrated by adjusting the blade metal angles to match the design pressure ratio. The corresponding predicted efficiency from the loss model was found to be in reasonable agreement.

1) Overall Fan Performance

The overall measured performance of the counter-rotating compressor is summarized in Figures 9 and 10, which respectively show the pressure ratio and efficiency as functions of corrected speed and corrected flow. The pressure ratio was derived by area-averaging the measured upstream/downstream spanwise pressure profiles. The reported efficiency was calculated from total enthalpy and entropy from NIST tables based on area-averaged total pressure and temperature [13,14]. The predicted APNASA performance was calculated from area-averaging the flow solution. Excluding the effect of the

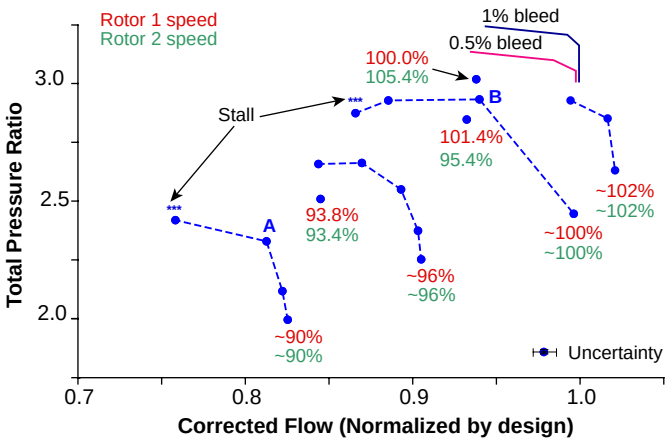

Figure 9: Compressor pressure ratio as predicted by APNASA (solid lines) and as measured (points).

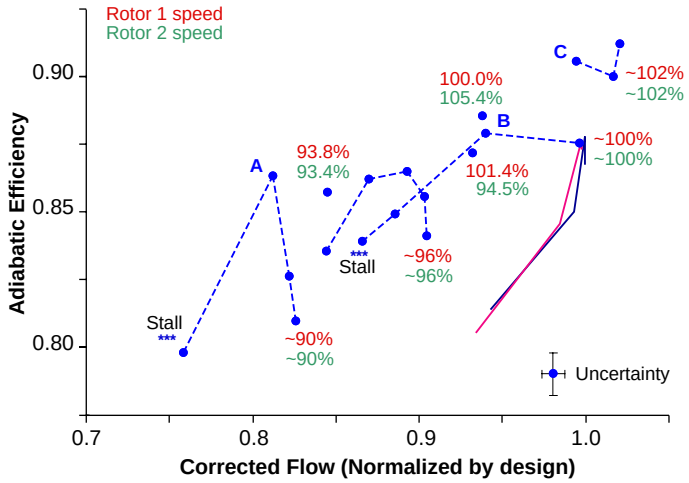

Figure 10: Adiabatic efficiency as predicted using APNASA (solid lines) and as measured (points).

boundary layers outside the radius of the hub and tip rake measurements resulted in an increase of about 0.3% in the predicted efficiency.

The nominal speeds of the two rotors as percent of the design speed are both shown (R1, top red and R2, bottom green). The design speed ratio between the rotors was maintained on each of the speedlines, and perturbations from the design speed ratio were tested at the individual points indicated on the map. The operating points on the speedlines were obtained by adjusting the downstream throttle setting. The APNASA calculations presented are all predictions made prior to the start of the test program. Because of the complexity of the dual-shaft test rig, it was difficult at first to set operating points to a precision greater than 2% in speed and mass flow prior to the test (although the precision improved with experience and there was no difficulty in reducing the data to 0.1% precision). The predictions were made at an inlet Reynolds number of 2.6×10^6 while tests were run at about 1.6×10^6 at design speed. The rotor tip clearance used in the

calculations was 0.6% and 0.9% of the tip chord for the first and second rotors respectively, while that in the tests is estimated to 60% lower than the calculation. The effect of the tighter clearance on the efficiency is estimated to be 0.6% increase based on the tip leakage model by Denton [15]. The result is that the CFD solutions are not exactly at the test conditions (resource limitations precluded rerunning the CFD at the measured operating points).

Figure 9 shows that the fan achieved a peak pressure ratio of 2.94 at design speed. This is 3% below the predicted design pressure ratio, and implies a difference of approximately 1% in the temperature ratio. Comparing this to the predicted peak efficiency points, the measured pressure ratio is 7% below the pressure ratio predicted for 1% aspiration, and 4% below the pressure ratio predicted for 0.5% aspiration. This implies a difference of approximately 2% between the measured and predicted temperature ratios. The one-dimensional fan model described above was used to relate the sensitivity of the stage temperature ratio or work to the flow angle deviation. The model indicated that the stage was very sensitive to changes in exit flow angles, and a rotor deviation change of approximately 1 degrees was sufficient to explain the observed differences in the measured and predicted performance. The increase in deviation may be caused by lower than design aspirated flow. An additional point to note is the strong coupling between the rotors due to absence of a stator, which typically constrains the absolute flow angle into a downstream rotor. Thus, in the counter-rotating compressor, a change in deviation of the first rotor will have a larger impact on the downstream rotor, and thus the overall stage performance than in a conventional multistage compressor.

The measured choking mass flow at the design speed is within 1% of the predicted design mass flow. The measurements show a flow range of 14% from choke to stall, which is approximately twice the range of the predicted speedline. Typical supersonic stages show a mass flow variation of about 7% at design speed conditions [9,16]. At 102% design speed, the measured choking mass flow is about 2% higher than design. This flow is determined solely by the choking mass flow in the first rotor and the increase in corrected flow is consistent with the speed increase of the first rotor. At 90% speed, the measured flow range from choke to stall is 10%, and the measured choking flow rate is within 2% of the value predicted by APNASA. It should be noted that the rotor geometry changes with mechanical speed; specifically, the stagger in supersonic fans increases as the blade speed drops, so the choking mass flow will drop as well. Variations in the geometry due to mechanical speed variations were not accounted for in the CFD calculations, which may explain the lower choking mass flow in the predictions.

The peak stage adiabatic efficiency measured was 91% (Figure 10). The variation in efficiency on the nominal design speedline (100% and 102% design speedlines), as the stage is throttled to stall, is qualitatively in agreement with the trend predicted by the APNASA calculation, although the lowest measured efficiency is about 3 percentage points higher than the lowest predicted efficiency. At 90% speed, only one efficiency prediction was available, and this is about 3 to 6 points lower

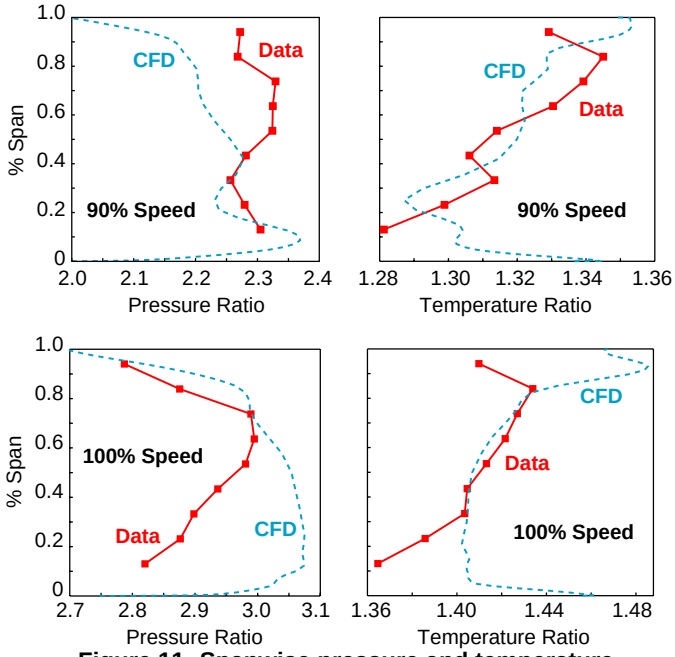

Figure 11: Spanwise pressure and temperature distributions.

than the measurement, depending on the operating point chosen for comparison.

The CFD and test data spanwise distribution of the rotor 2 exit temperature and pressure are given in Figure 11 for point B on the 100% speedline and point A on the 90% speedline. At 100% speed, the CFD over predicts the pressure rise along the inner half of the span while under predicting the temperature rise. At 90% speed, the outer span pressure rise is over predicted.

Given the sensitive supersonic operating condition of both rotors, the measured and predicted performance are in good agreement. Thus, we conclude that the overall aspirated compressor aerodynamic design system gives useful results even in new and unusual sectors of design space such as that selected for this fan.

2) Casing Static Pressure Measurements

In the tests to date, the outer casing static pressure measurements provide the only independent assessment of the performance of the first rotor. At the choking mass flow on the nominal design speed, where the first rotor is choked, the measured ratio of wall static to upstream total pressure is 1.39 while the value predicted by APNASA is 1.41. At the stall point, the measured static pressure ratio is 1.45 and the predicted value at the last computed point is 1.44. At 90% speed, the measured normalized static pressure is 1.3 and the predicted value is 1.31. This comparison indicates that this measure of first rotor performance is in agreement with prediction at both speeds.

3) Speed Ratio Perturbations

Although the stage was nominally designed and tested for a speed ratio of 0.8, changes in the speed ratio will occur in an

engine environment. Two speed ratio perturbations were examined about point B on the compressor map. Increasing the speed of the second rotor while maintaining the speed of the first rotor results in an increase in pressure ratio and efficiency. The second rotor effectively acts as a throttle for the first rotor, so increasing the speed ratio moves the operating point of the first rotor closer to choke. This can be seen in the decrease in the normalized static pressure downstream of the first rotor shown in Table 4. It is interesting to note that the overall flow rate does not change even though the first rotor is being throttled down. This unusual behavior can be explained by noting that an increase in the exit deviation of rotor 1, caused by throttling down, can change the absolute flow angle without necessarily changing the axial velocity (mass flow). The overall result is that the inlet corrected flow of rotor 2 can change as the blade speed is increased without changing the overall mass flow rate of the compressor. This behavior does not occur in a conventional stage since the stators constrain the absolute flow angles into downstream rotors.

Table 4: Comparison of casing static pressures at speed ratio perturbations about the design speed

% Speed	Rotor 1	Rotor 2	Overall
100-100	1.41	1.82	2.57
100-105	1.38	1.89	2.61
101-95	1.46	1.73	2.52

Conversely, decreasing the speed ratio results in throttling up of the first rotor, moving it closer to stall. The static pressure rise downstream of the first rotor at 100-95% speeds is greater than the normalized static pressure at the stall point of the stage at the design speed ratio. The key point is that changes in speed ratio can have a large impact on the stage performance, in particular of the first rotor. The design implication is that the first rotor must be designed with the appropriate stall margin to withstand the throttling effect caused by reductions in the speed ratio in an engine environment.

4) Stall Behavior

As is common practice, high frequency response pressure measurements on the outer casing downstream of the stage were used to detect rotating stall. The quasi-steady test window contains about 20 revolutions of the first rotor and 16 revolutions of the second rotor. Stall was detected during the test time for operating points with a sufficiently closed throttle. The rotating stall frequency observed was approximately 35% of the first rotor speed.

Figure 12 show the measured stall margin of the fan as defined in [9]. The stalling pressure ratio was taken as the last operating point on each speedline. (Note, that stall was not observed on the 95% and 102% speediness, so these are excluded from this discussion) The fan exhibits a stall margin of at least 25% on the three speedlines depending on the operating pressure ratio. The stall margin at peak efficiency on the speedlines is approximately 12%. At the nominal design speed, the stall margin is 15% at a pressure ratio of 2.8 and

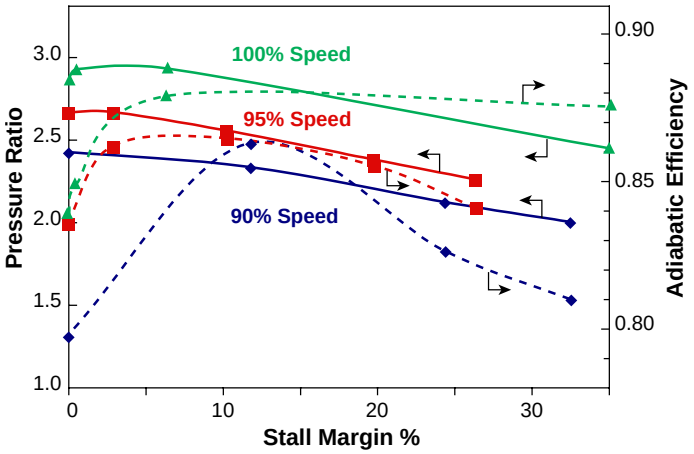

Figure 12: Measured stall margin vs. pressure ratio.

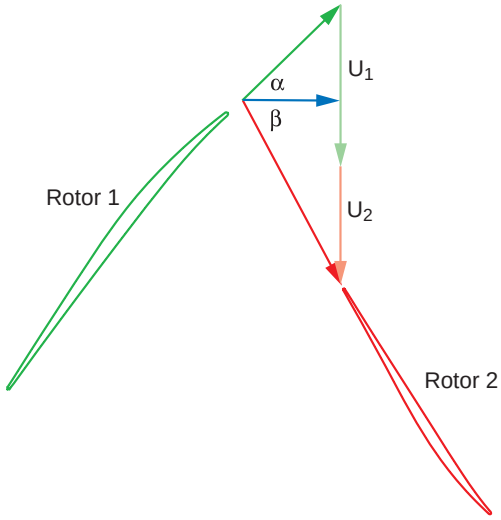

Figure 13: Velocity triangles in the frame of reference of the first rotor.

adiabatic efficiency of 88%.

This is the first counter-rotating fan reported in the literature and, for a high pressure ratio supersonic fan, this stage has considerable flow range and stall margin. This behavior merits some examination. Cumpsty [17] presents a simple explanation that a steeper pressure rise characteristic smoothes out non-uniformities in the flow and therefore is advantageous in delaying stall. The slope of the ideal characteristic of a vaneless counter-rotating fan is:

$$\frac{\partial \psi}{\partial \phi_{inlet}} = -\left(\frac{U_2}{U_1}\right)\tan(\alpha) - \left(1 - \frac{U_2}{U_1}\right)\tan(\beta) \cdot$$

Here, U is the blade speed, α is the relative exit angle of rotor 1, and β is the blade relative inlet angle of rotor 2. For simplicity, it is assumed that there is no inlet swirl and the axial velocity is constant. Substituting appropriate flow angles

and speeds (note that U_1 and U_2 are defined with opposite signs here) in this equation shows that a counter-rotating fan such as this has at least a 50% steeper characteristic compared to a conventional 2-stage compressor with the same average work coefficient.

A similar conclusion can be drawn by using the analysis of Smith [18] who showed that a rotor with a sum of absolute and relative angles ≥90 degrees has a greater ability to damp incoming total pressure disturbances. Such a combination of flow angles also results in a region of high loss in one frame of reference becoming a region of excess stagnation enthalpy in the frame of reference downstream. The second rotor of the counter-rotating fan exhibits this condition when viewed from the frame of reference of the upstream rotor as shown in Figure 13 (the sum of the angles at the meanline is approximately 110 degrees). Thus, the second rotor will reduce an incoming stall cell or total pressure disturbance from the first rotor potentially extending the operating range of the stage.

5) Comments on Stage Efficiency

The data and CFD efficiency presented in Figure 10 and subsequent discussion is that for the rotor 2 exit flow (the "through flow") in the area mapped by the instrumentation rakes. As can be seen in Figure 11, this excludes the hub and tip endwall flows. Using the CFD solutions as a guide, inclusion of these flows reduces the overall efficiency by about 0.3 %. Also as noted, the tests were run at relatively tight tip clearances, so that opening up the clearances to the values used in the CFD calculations would add an additional 0.6% in loss. Taken together, these imply that the measured through flow efficiency should be debited by 0.9%. In this case the, the peak efficiency on the 100% speed line would be 87% while the 102% speedline reaches 90%.

An engine designer is concerned with more than the compressor through flow efficiency and must consider all of the power debits on the compressor, which includes the rotor 2 bleed flow. In this experimental design, the bleed flow is taken radially inward through the blades and disk and so recovers some of its energy since this configuration behaves as a radial inflow turbine. However, the bleed fluid suffers total pressure drops in passing thorough the choked bleed slot on the blade surface, in the passage within the blade and disk, and in deswirling into the stationary frame. We have estimated (but not measured) the net effect of these factors to be the equivalent of about a 0.5% loss in efficiency. More careful design of the bleed system may reduce this loss by, for example, not choking the bleed slot and reducing the internal passage Mach numbers. If this bleed air is used elsewhere in the engine, the importance of this penalty would decrease.

CONCLUSIONS

This study is the first public report of the detailed aerodynamic design and test of a vaneless counter-rotating compressor stage. In this design, aspiration on the second rotor enabled high loading at a low rotor mechanical speed compatible with high Mach number flight. The authors conclude from the study:

1) With aspiration on the second rotor, a counter-rotating vaneless fan has met nominal design objectives of a pressure ratio of 3:1 with rotor speeds of 1450 and 1150 fps on the first and second rotors, and an adiabatic efficiency of better than 87 percent.
2) The aerodynamic design approach developed on this, and two previous aspirated compressors, is capable of producing aerodynamic designs for aspirated compressors for new and unique design requirements for which there is no prior experimental experience.
3) Blowdown testing is a practical and low-cost approach to verification of new and unusual compressor designs.
4) Vaneless counter-rotating compressors may offer high efficiency, lightweight solutions to compression system requirements.

Clearly more research can and should be done on counter-rotating designs before development. This work would include expanding the test and analysis envelope to include a complete engine operating map, assessment of mechanical robustness criteria such as deterioration and aeromechanics, and, for aspirated implementations, integration of the compressor bleed with the engine secondary flow system.

ACKNOWLEDGMENTS

This research was funded by DARPA and the US Air Force Office of Scientific Research. GE Aircraft Engines collaborated in the early phases of the design. TURBOCAM of Dover NH fabricated the stage. Kulite Semiconductor Products provided the pressure instrumentation.

REFERENCES

1. Schuler, B.J., Kerrebrock, J.L., and Merchant, A., "Experimental Investigation of an Aspirated Fan Stage", *Journal of Turbomachinery*, Vol. 127, No. 2, pp. 340-348, April 2005.
2. Merchant, A., Kerrebrock, J.L., Adamczyk, J.J., and Braunscheidel, E., "Experimental Investigation of a High Pressure Ratio Aspirated Fan Stage," *Journal of Turbomachinery*, Vol. 127, No. 1, pp. 43-51, January 2005.
3. Merchant, A.A., "Design and Analysis of Axial Aspirated Compressor Stages," PhD Thesis, Massachusetts Institute of Technology, Cambridge, MA, June 1999.
4. Johnson, J. E., "Variable Cycle Engine Developments at General Electric – 1955-1995," AIAA, 1995.
5. Brear, M.J., Kerrebrock, J.L., Epstein, A.H., "Propulsion System Requirements for Quiet, Long Range, Supersonic Aircraft," Paper FEDSM2003-45690, *Proc. of FEDSM'03*, 4th ASME/JSME Joint Fluids Engineering Conference, Honolulu, HI, July 2003.
6. Merchant, A., Epstein, A.H., and Kerrebrock, J.L., "Compressors with Aspirated Flow Control and Counter-Rotation,"AIAA-2004-2514, 2nd AIAA Flow Control Conference, Portland, Oregon, June 28-1, 2004.
7. Kirtley, K. R., Graziosi, P., Wood, P., Beacher, B. and Shin, H., W., " Design and Test of an Ultra-Low Solidity

Flow-Controlled Compressor Stator," ASME Paper 2004-GT-53012.
8. Adamczyk, J.J., "Model Equation for Simulating Flows in Multistage Turbomachines," ASME Paper 85-GT-226, 1985.
9. Wadia, A.R., Szucs, P.N., Crall, D.W., "Inner Workings of Aerodynamic Sweep," *Journal of Turbomachinery*, Vol. 120, pp. 671-682, October 1998.
10. Wadia, A.R. and Copenhaver, W.W., "An Investigation of the Effect of Cascade Area Ratios on Transonic Compressor Performance," *ASME Journal of Turbomachinery*, Vol. 118, 1996, pp 760-770.
11. Kerrebrock, J.L., "The MIT Blowdown Compressor Facility, " MIT Gas Turbine Laboratory Report No. 108, September, 1975.
12. Keogh, R.C., Guenette, G.R., Sommer, T.P., "Aerodynamic Performance Measurements of a Fully-Scaled Turbine in a Short Duration Facility," ASME IGTI 2000-GT-486.
13. Parker, D. "Design and Operation of a Counter-Rotating Compressor Blowdown Test Facility"", SM Thesis, Massachusetts Institute of Technology, Cambridge, MA, June 2005.
14. Onnee, J-F, "Aerodynamics Performance Measurements in a Counter-Rotating Aspirated Compressor," SM Thesis, Massachusetts Institute of Technology, Cambridge, MA, June 2005.
15. Denton, J.D., "Loss Mechanisms in Turbomachines," *Journal of Turbomachinery*, Vol 115, pg 621-656, October 1993.
16. Wennerstrom, A.J., "Experimental Study of a High-Throughflow Transonic Axial Compressor Stage," *ASME Journal of Engineering for Power*, Vol. 106, pp.553-559, July 1984.
17. Cumpsty, N.A., *Compressor Aerodynamics*, Longman, UK, 1989.
18. Smith, L.H., " Recovery ratio—a measure of the loss recovery potential of compressor stages," *Trans. ASME*, Vol. 80, pp. 3, 1958.
19. Kerrebrock, J.L. "The Prospects for Aspirated Compressors," AIAA-2000-2472, Denver, CO, June, 2000.